

The coupled physical-new production system in the equatorial Pacific during the 1992–1995 El Niño

Anne Stoens,¹ Christophe Menkès,¹ Marie-Hélène Radenac,¹ Yves Dandonneau,¹
Nicolas Grima,¹ Gérard Eldin,^{2,3} Laurent Mémerly,¹ Claudie Navarette,²
Jean-Michel André,² Thierry Moutin,⁴ and Patrick Raimbault⁴

Abstract. We investigate the coupling between the physics and new production variability during the period April 1992 to June 1995 in the equatorial Pacific via two cruises and simulations. The simulations are provided by a high-resolution Ocean General Circulation Model forced with satellite-derived weekly winds and coupled to a nitrate transport model in which biology acts as a nitrate sink. The cruises took place in September–October 1994 and sampled the western Pacific warm pool and the upwelling region further east. The coupled model reproduces these contrasted regimes. In the oligotrophic warm pool the upper layer is fresh, and nitrate-depleted, and the new production is low. In contrast, the upwelling waters are colder, and saltier with higher nitrate concentrations, and the new production is higher. Along the equator the eastern edge of the warm pool marked by a sharp salinity front, also coincides with a "new production front". Consistent with the persistent eastward surface currents during the second half of 1994, these fronts undergo huge eastward displacement at the time of the cruises. The warm/fresh pool and oligotrophic region has an average new production of $0.9 \text{ mmol NO}_3 \text{ m}^{-2} \text{ d}^{-1}$, which is almost balanced by horizontal advection from the central Pacific and by vertical advection of richer water from the nitrate reservoir below. In contrast, the upwelling mesotrophic region shows average new production of $2.1 \text{ mmol NO}_3 \text{ m}^{-2} \text{ d}^{-1}$ and the strong vertical nitrate input by the equatorial upwelling is balanced by the losses, through westward advection and meridional divergence of nitrate rich waters, and by the biological sink.

1. Introduction

The major focus of the Joint Global Ocean Flux Study (JGOFS) international program is devoted to the oceanic carbon cycle and its long-term consequences on the variations of the atmospheric CO_2 content. Among JGOFS process studies, those concerning the equatorial Pacific were undertaken for several reasons.

First of all, the equatorial cold tongue of upwelled waters has large spatial extension [Wyrtki, 1981]. These waters upwelled from depth are rich in nutrients and in inorganic carbon. High nutrient content enhances photosynthesis, new production of organic carbon, and sedimentation of particles. In addition, the high carbon content of the upwelled waters maintains a high partial pressure of CO_2 at the sea surface. In relation to this, in this region the CO_2 flux at the air-sea interface goes to the atmosphere, and the Pacific equatorial upwelling is the largest marine source of CO_2 to the atmosphere [Tans *et al.*, 1990]. This makes the equatorial Pacific a key region for the carbon cycle.

A second characteristic of the equatorial Pacific is its relatively modest chlorophyll content and low primary productivity compared to the abundance of nitrate in the surface layers. The equatorial Pacific upwelled waters have thus been described as high nutrients-low chlorophyll waters (HNLC) [Thomas, 1979] and the roles of iron [Martin, 1990; Barber, 1992] or of grazing [Walsh, 1976] have been proposed to explain this paradox. However, neither the high carbon fluxes to the atmosphere and to depth, which are common to all tropical upwelling areas, nor the HNLC character, which is also observed in the Antarctic, are exclusive of the equatorial Pacific.

In contrast, a third property is unique to this region: it arises from the interannual El Niño–Southern Oscillation (ENSO) that affects the world climate. During the warm phases of this oscillation (El Niño) the equatorial upwelling collapses dramatically reducing the biological sink of carbon associated with new production [Barber and Chavez, 1983; Dandonneau, 1986] and the CO_2 outgassing [Wong *et al.*, 1984, 1993; Feely *et al.*, 1995; Dandonneau, 1995]. The study and prediction of ENSO constituted the major goals of the 1985–1994 international Tropical Ocean Global Atmosphere program (TOGA). In the course of TOGA our general knowledge of large-scale circulation has been greatly improved. It is now well known that the variability of the equatorial Pacific results from basin-wide coupling processes between the ocean and the atmosphere. The circulation of surface water masses, which controls the equatorial upwelling, is deeply affected by these processes. This emphasizes the point that the value of biogeochemical variables at a given position, which results largely from the

¹ Laboratoire d'Océanographie Dynamique et de Climatologie, (CNRS/ORSTOM/Univ. Paris 6), Paris, France.

² Institut Français de Recherche Scientifique pour le Développement en Coopération, Nouméa, New Caledonia, France.

³ Now at Laboratoire d'Etudes en Géophysique et Océanographie Spatiales, Toulouse, France.

⁴ Centre d'Océanologie de Marseille, Marseille, France.

advection of upwelled water, is controlled by these processes and thus cannot be properly understood in a one-dimensional (1-D) view. In particular, horizontal advection is of primary importance for determining the biogeochemical conditions in the equatorial Pacific. This complicates the study of the biological fluxes to such a point that certainly, the JGOFS study of the equatorial Pacific would not have been possible without the lessons from TOGA.

During this program, in situ observational networks such as Tropical Atmosphere Ocean (TAO) have been deployed all over the equatorial Pacific, which deliver, in particular, real-time knowledge of the subsurface thermal structure variations of the ocean (10°S-10°N) and knowledge of the current along the equator [Hayes *et al.*, 1991, McPhaden, 1993] so that the equatorial Pacific Ocean is now the best observed ocean. Therefore the international JGOFS study of the equatorial Pacific has benefited from the attainments of TAO. For example, Kessler and McPhaden [1995] used these networks to describe of the dynamical aspects of the equatorial Pacific during the period of the U.S.-JGOFS EqPac cruises which sampled the central Pacific Ocean, at 140°W, during a warm anomaly, and during near-normal conditions in spring and fall of 1992 respectively.

The western equatorial Pacific has been studied during an Australian-JGOFS cruise in October 1990 [Mackey *et al.*, 1995] during non El-Niño conditions. The FLUPAC and OLIPAC JGOFS-France cruises in the western to central equatorial Pacific were made in September-November 1994 when conditions were more characteristic of warm conditions. The latter cruises sampled the ocean in dynamically and biogeochemically contrasted areas. In short, the western equatorial Pacific is characterized by a warm pool region where surface waters are warmer and fresher than upwelled waters farther east. This warm pool experiences huge zonal excursions on interannual timescales which are of fundamental importance for the world climate [Picaut *et al.*, 1996]. The signature of these two contrasted physical regimes is also reflected in biogeochemistry as seen in Figure 1 where abundance of 0-500 m integrated mesozooplankton (>200 µm) [Le Borgne and Rodier, 1997] as well as other parameters along the equator during FLUPAC increase sharply from the warm pool region to the upwelling region. This suggests a strong coupling between the physics and biogeochemistry at the time of the FLUPAC and OLIPAC cruises.

The main objective of this work is thus to gain knowledge on the coupled dynamical-biogeochemical processes that are at work in the settling, in the maintenance, and in the large-scale displacement of the nutrient poor warm pool and the adjacent waters in relation to ENSO conditions. Thus we aim at understanding the main coupled factors that control new production in the equatorially contrasted waters.

Such knowledge can be gained through observations: for instance, the FLUPAC and OLIPAC cruises were focused on the estimation of new and exported primary production, in relation to the dynamics of the ocean. However, as useful as it may be, such information provided by the FLUPAC and OLIPAC data is only relevant to the place and time where these cruises took place. In order to understand the observations in the large-scale context, it is necessary to enlarge the scope of the punctual cruises to the basin and to the seasonal to interannual scales. While synoptic view of the ocean sea level variations is successfully given by altimeters

such as TOPEX/POSEIDON [Busalacchi *et al.*, 1994; Picaut *et al.*, 1995] and dynamic height is monitored by the TAO network, previous attempts to develop such a comprehensive data set for biogeochemical data are limited to satellite-detected sea color by the Coastal Zone Color Scanner [Yoder *et al.*, 1993] and monitoring using measurements by ships of opportunity [Dandonneau, 1992]. Therefore the basin-scale link between the physics and the biology can only be inferred from coupled models.

In the equatorial ocean where advection processes, especially by zonal currents, are known to be important [Picaut and Delcroix, 1995], 1-D coupled models can generally not account for observed variations, and one needs to use a 3-D coupled model to describe the complexity of observed variability. Coupled biological-physical models in the equatorial Pacific have already been used to study the seasonal variations of the basin and long-term evolution [Toggweiler and Carson, 1995; Chai *et al.*, 1996]. Toggweiler and Carson, and Chai *et al.* used climatological forcing in their simulations which is not appropriate for a case study focused on the situation encountered at the time of FLUPAC and OLIPAC or for understanding the coupled conditions during ENSO period. Similarly, it is not well suited for the study of transient processes such as equatorial and instability waves which propagate in the equatorial region and may deeply impact the biology [Murray *et al.*, 1994].

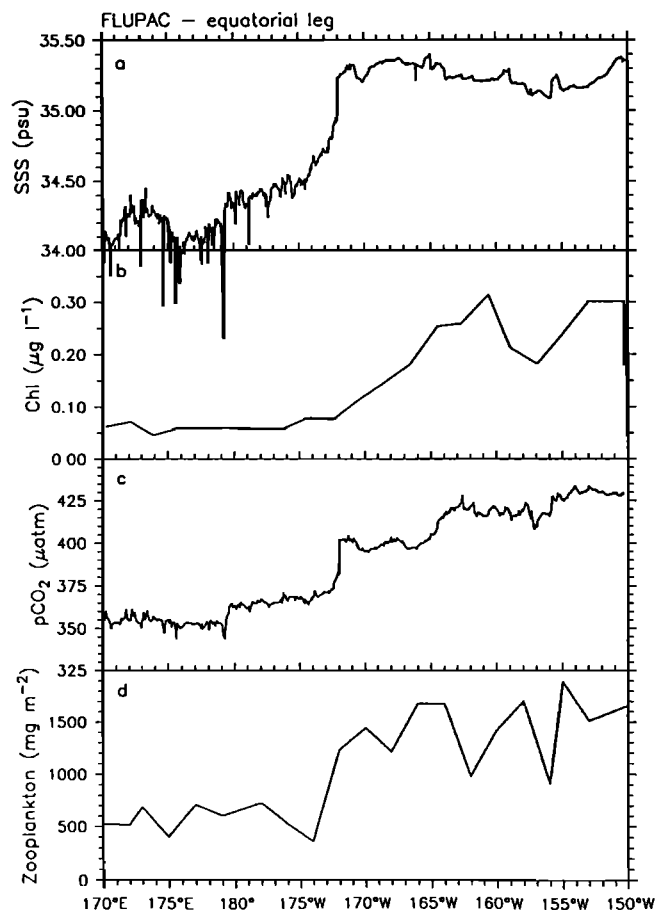


Figure 1. Surface biogeochemical measurements along the equatorial FLUPAC leg: (a) sea surface salinity, (b) chlorophyll, (c) $p\text{CO}_2$ in the ocean, and (d) ash free dry weight of mesozooplankton in the upper 500 m adapted from Le Borgne and Rodier, [1997].

In order to explicitly resolve all these features we use here the high-resolution Ocean General Circulation Model (OGCM) OPA of the Laboratoire d'Océanographie Dynamique et de Climatologie (LODYC) [Blanke and Delecluse, 1993] forced by high-resolution, high-quality remotely sensed European Remote Sensing (ERS)-1 scatterometer stresses [Grima et al., 1998] and coupled to a nitrate transport model. By this we aim at simulating the physical-new production interactions during the 1992-1994 weak El Niño period in which FLUPAC and OLIPAC took place.

The paper is thus organized as follows: in section 2, data and model descriptions are given. In section 3 a quick overview of the large-scale variations of the physical conditions from 1992 to 1995 is given from data and model fields. The coupled dynamical-biogeochemical modeled situations during the FLUPAC and OLIPAC cruises are then compared to data. In section 4 the variations of coupled dynamical-new production features over the equatorial Pacific from 1992 to 1995 are studied using the model. It is shown that new production at the equator experiences a sharp transition when going from the warm/fresh pool region to the upwelling region and that this transition has large east-west displacements over the basin in association with the ENSO-related east-west displacements of the salinity front at the eastern edge of the warm pool. Finally, discussion about the modeled new production is given, and in section 5 the conclusion is presented.

2. Data and Model

2.1. Materials and Methods Used During FLUPAC and OLIPAC Cruises

The FLUPAC cruise sampled the equatorial Pacific in these two different regimes with a meridional transect along 165°E (20°S-6°N; September 1994), across the oligotrophic waters of the warm pool, and an equatorial section across the eastern edge of the warm pool into the upwelling region (167°E-150°W; October 1994). The OLIPAC meridional transect took place along 150°W (13°S-1°N; November 1994).

Temperature and salinity were obtained using a Sea-Bird SBE 911+ Conductivity-Temperature-Depth profiler (CTD). The sensors were calibrated before the beginning of FLUPAC, and salinity data were validated after measurements of discrete samples with a Portasal salinometer. The vertical profiles of temperature and salinity were processed for spike removal and binned every meter using the software provided by Sea-Bird.

Currents were continuously recorded by two acoustic Doppler current profilers (ADCPs) from R. D. Instruments. The two ADCPs used 75 and 300 kHz frequencies, with vertical resolutions of 16 and 4 m and first bins at 28 and 12 m, respectively. The results from the two instruments were in good agreement, so that the two files of data could be merged into a single set of vertical profiles from 12 to 700 m depth.

Nitrate was measured with a Technicon autoanalyzer using the colorimetric method described by Strickland and Parsons [1972]. For low nitrate concentrations this method was improved to detect nitrate at concentrations as low as 0.003 $\mu\text{mole kg}^{-1}$ at FLUPAC [Oudot and Montel, 1988] and 0.001 $\mu\text{mole kg}^{-1}$ at OLIPAC [Raimbault et al., 1990].

The chlorophyll concentration was measured according to several techniques (including high-performance liquid chromatography and spectrofluorometry). The data presented here, in order to provide an indication of the biological activity, were obtained using the fluorescence/acidification technique described by Yentsch and Menzel [1963], where the pigments are extracted by methanol instead of acetone [Herbland et al., 1985]. Filtration was made on Whatman GF/F filters, filtration pressure being kept below 0.15 atm.

2.2. Data From Observations Networks

Among diverse observing systems enhanced or developed during TOGA the TAO array of deep ocean moorings provides a permanent and synoptic view of the upper ocean thermal structure with high temporal resolution. Dynamic heights deduced from the TAO data were kindly provided by M. McPhaden and D. McClurg at Pacific Marine Environmental Laboratory (PMEL), National Oceanic and Atmospheric Administration (NOAA). These dynamic heights at mooring positions are interpolated onto a regular 5° longitude \times 1° latitude \times 1 day grid using objective analysis used in Menkes et al. [1995]. Together with these in situ data, the Reynolds and Smith [1994] sea surface temperatures (SSTs) are used.

2.3. The Dynamical Model

The dynamical model we are using is the three tropical oceans version of the OPA-LODYC OGCM [Maes et al., 1997]. One specificity of this model is the parameterization of vertical diffusion using the 1.5 turbulent kinetic energy (TKE) closure [Blanke and Delecluse, 1993]. This high-resolution (45' longitude \times 20' latitude at the equator; 16 vertical levels in the upper 150 m) model is forced with observed weekly stresses deduced from ERS-1 scatterometer [Grima et al., 1998]. There is a good agreement between wind vectors from the ERS-1 scatterometer and winds measured on the TAO buoys [Bentamy et al., 1996; Grima et al., 1998].

To drive the OGCM "OPA7," satellite-derived wind stresses are completed with water and heat fluxes. These fluxes are computed using bulk aerodynamic formulae with stress from ERS-1, Reynolds and Smith's [1994] SSTs, and all other parameters derived from the atmospheric model Arpège-Climat [Dequé et al., 1994] outputs. The OGCM has been forced from mid-1992 to 1995. Overall comparisons between the outputs of the ERS-1 forced OGCM, TAO in-situ data, and satellite observations have been performed for different ocean variables over the equatorial Pacific Ocean [Grima et al., 1998]. Five-day outputs were analyzed spanning the 1992-1995 period, and during the specific period of FLUPAC and OLIPAC, linear interpolation of five-day outputs to daily values was performed for comparison with data.

2.4. The Coupled Biogeochemical Model

This OGCM is coupled to an off-line tracer nitrate model using the dynamical outputs to solve the advection-diffusion equations [Levy, 1996] on the OGCM grid:

$$\frac{\partial \text{NO}_3}{\partial t} = -(\mathbf{u} \cdot \nabla) \text{NO}_3 + K_h \Delta \text{NO}_3 + \partial_z (K_z \partial_z \text{NO}_3) + \left(\frac{\partial \text{NO}_3}{\partial t} \right)_{\text{biology}} \quad (1)$$

The left-hand term represents the eulerian variation of the tracer (nitrate) and is calculated as the sum of the advection terms (first term in the right-hand side), the horizontal diffusion terms (this one is quasi-negligible here), vertical diffusion terms, and the biological sink. Currents and diffusion coefficients are taken from the dynamical simulation. The last term represents the biological nitrate sink (biological model). As in the host physical model, the governing equations are solved on a C grid. An absolute requirement is that the biological tracer concentrations remain positive. Therefore a positive definite advection transport scheme [Smolarkiewicz and Clark, 1986] is used to compute advection.

Previous attempts to represent the biogeochemistry in the equatorial Pacific [Toggweiler and Carson, 1995; Chai et al., 1996] were based on a biological model where the phytoplankton, the zooplankton, ammonium, and detritus were explicit compartments where the nitrogen fixed by photoautotrophs could accumulate. However, the field data and experimental knowledge to initialize these compartments and adjust the fluxes between each other are uncertain. Since we focus here on new production [Dugdale and Goering, 1967] we choose to reduce the ecosystem to a single nitrate compartment. Thus, in this simple system the new nitrate that is taken by the photoautotrophs cannot be stored in any compartment in the photic layer and must then be immediately remineralized at depth. This procedure presents the inconvenience of a too strict coupling between new production and remineralization that does not account for the natural storage into biomass or dissolved organic nitrogen and for the transport of stored nitrogen before remineralization. It was adopted, however, for its simplicity and ability to represent the variability of the nitrate field at the time of FLUPAC and OLIPAC.

New production is carried out by the phytoplankton, and thus its rate is biomass-dependent. It is also limited by the availability of light and nutrients. Limitation by light in our model is made according to Kiefer and Mitchell [1983]. The photosynthetic radiation incident at the surface is provided by the radiative flux used to force the dynamical model. Since our model does not include a phytoplankton compartment a special procedure had to be developed to estimate its biomass, or chlorophyll concentration, at a given place and time. The synthesis of the satellite Coastal Zone Color Scanner (CZCS) sea color data [Yoder et al., 1993], as well as a 10 year monitoring experiment using ships of opportunity [Dandonneau, 1992], shows that the chlorophyll concentration at the surface decreases slowly from the eastern equatorial upwelling to the tropical waters to the north, to the south, or to the west (warm pool). Similarly, a large-scale decrease in the nitrate concentration and an increase in temperature are observed [Chavez et al., 1996]. The FLUPAC and OLIPAC data also confirm that higher chlorophyll concentrations respond to higher nitrate concentrations. Given this, it is possible to derive an empirical linear relationship between the nitrate surface data and chlorophyll surface data (such a relationship was computed using the FLUPAC, OLIPAC, and the EqPac data) and to compute at each model time step the chlorophyll concentration at the surface. The vertical profile of chlorophyll is then rebuilt starting from the chlorophyll concentration at the surface propagated vertically via statistical equations by Morel and Berthon [1989]. Once a

chlorophyll field is calculated, new production can be computed according to

$$\left(\frac{\partial \text{NO}_3}{\partial t}\right)_{\text{biology}} = -V_{\text{max}} \frac{\text{NO}_3}{\text{NO}_3 + K_{\text{NO}_3}} \frac{\text{PUR}}{\text{PUR} + K_E} [\text{Chl}] \quad (2)$$

where V_{max} is the maximum nitrate assimilation rate ($\mu\text{mol NO}_3 \text{ mg Chl}^{-1} \text{ s}^{-1}$) and K_{NO_3} is the half saturation concentration ($\mu\text{mol NO}_3 \text{ kg}^{-1}$). The V_{max} and K_{NO_3} values which give the best fit with the FLUPAC and OLIPAC observations of nitrate concentration are $4 \times 10^{-3} \mu\text{mol NO}_3 \text{ mg Chl}^{-1} \text{ s}^{-1}$ and $0.01 \mu\text{mol NO}_3 \text{ kg}^{-1}$, respectively. These parameters set a Michaelis-Mentens-type limitation to the nitrate sink according to MacIsaac and Dugdale [1969]. PUR is the photosynthetic usable radiation ($\text{mol photons m}^{-2} \text{ s}^{-1}$) [Morel, 1991] deduced from the short wave downward radiation and a phytoplankton light absorption scheme based on a two wavelength (red and blue) light absorption spectrum (J. Ballé, personal communication, 1998). The daily cycle of irradiance is not represented in this model, and K_E (i.e., the half-saturation constant for PUR) is taken to be equal to $70 \times 10^{-6} \text{ mol photon m}^{-2} \text{ s}^{-1}$ in order to reproduce a limitation by light in agreement with the results of light-photosynthesis experiments made by K. Allali and M. Babin during FLUPAC and OLIPAC [Moutin and Coste, 1996].

The parameters V_{max} and K_{NO_3} which control this nitrate sink are the same over the basin as if a phytoplankton population with constant physiological properties occupied the studied area. This simplified representation of the biology in a domain which is nitrate-limited in the warm pool and subtropical gyres and nitrate-rich in the equatorial HNLC region does not disagree with the conclusions of Landry et al. [1997], who do not observe any fundamental difference in the characteristics of the phytoplankton populations between these two regimes. Using a unique set of constants for nitrate assimilation kinetics all over the basin can be justified by the fact that nitrate is not the primary limiting factor in the equatorial Pacific. In fact, iron limitation is effective everywhere [Price et al., 1994]. As a consequence, nitrate fixation is mostly dependent on biomass, and limitation by nitrate occurs only when the nitrate concentration is less than K_{NO_3} .

The computation of the nitrate sink is made down to the depth of the photic layer. New production is then instantaneously exported as particles below the photic layer with an exponential decrease, and remineralized, as by Honjo [1978]. The constant for the exponential decrease of remineralization with depth was fixed to 120 m, a value which fits best with the sediment traps data from the EqPac cruises [Murray et al., 1995].

The model was initialized on April 20, 1992, with nitrate concentrations from Levitus climatology. The initial nitrate field is clearly not in equilibrium with the large-scale dynamics of the equatorial Pacific at this time, especially in the surface layer (indeed, warm pool nitrate concentrations in the Levitus climatology are seemingly too high). In order to achieve equilibrium the biological model was spun up by rerunning a perpetual April 1992 to March 1993 year five times. After this 5 year spin up the nitrate field was in nearly equilibrium with the physics of the model, the integrated amount of nitrate in the photic layer increasing by only 3%

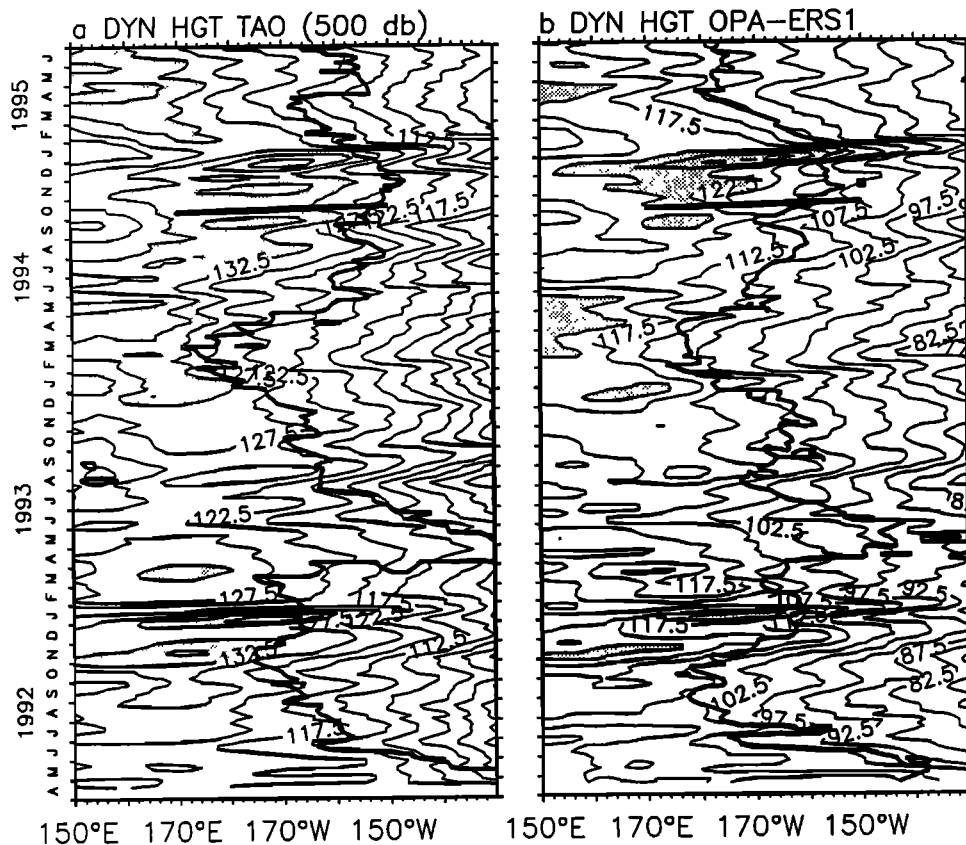


Figure 2. (a) Equatorial section of observed Tropical Ocean Global Atmosphere (TOGA)- Tropical Atmosphere Ocean (TAO) and (b) OPA-European Remote Sensing (ERS)-1 modeled dynamic heights. These dynamic heights are referenced to 500 dbar. Areas of pronounced dynamic height pulses are shaded. The 28°C observed isotherm [Reynolds and Smith, 1994] and the modeled 28°C isotherm are superimposed on Figures 2a and 2b, respectively. The FLUPAC equatorial transect is superimposed as a dark line in September-October 1994, and the OLIPAC cruise is represented by a dot at 150°W in November 1994.

during the fifth year. The model was then forced with the 1992-1995 dynamical simulation, and results are then examined from mid-April 1992 to June 30, 1995. From 15° to 20°S and 15° to 20°N the modeled nitrate is smoothly relaxed to Levitus climatology. At the western and eastern boundaries a similar but stronger relaxation is imposed in order to remedy abnormally strong vertical advection of nitrate due to unrealistic vertical motions near America's and Papua New Guinea's coasts in the dynamical model. This procedure, however, did not affect the dynamic or biological nitrate fluxes at 165°E where the model results are compared to the observations. The biological model is active down to 1260 m depth where nitrate concentrations are relaxed to Levitus climatology.

3. Dynamical and Biogeochemical Fields: Data and Model Comparisons

3.1. The Equatorial Pacific in 1992-1995

An equatorial section deduced from TOGA-TAO and modeled dynamic heights (referenced to 500 dbar) is presented in Figure 2 together with the observed and modeled 28°C isotherm position for the period. The 28°C isotherm position is an indicator of the position of the eastern edge of the warm pool [Picaut *et al.*, 1996]. The equatorial section of

the modeled dynamic height (Figure 2b) shows a -10 cm systematic mean bias with respect to the observations (Figure 2a). Reasons for this are unclear at present and merit further investigations. However, as in the observations, time varying features such as Kelvin pulses are in very good agreement.

The period from 1991 to 1994 is characterized by three successive weak warm events that resulted in a long-lived warm anomaly in the equatorial Pacific [Goddard and Graham, 1997]. During that time the Southern Oscillation Index (SOI) remained negative [National Oceanic and Atmospheric Administration (NOAA), 1994]. Kessler and McPhaden [1995] described the period 1991-1993 during which the U.S.-JGOFS EqPac cruises took place. Abnormally high temperature and low productivity representative of El Niño conditions prevailed during the spring cruise as can be seen here from the 28°C isotherm eastward positions (Figures 2a-2b). In contrast, the fall cruise was conducted when near normal conditions associated with a brief return of moderate easterlies were back [Murray *et al.*, 1995] as indicated by 28°C positions near the dateline both in data and model. From October up to December 1992, seasonal occurrences of westerly wind bursts were observed that are seen both in the data and the model to generate downwelling Kelvin waves. These propagate to the east in association with the warm pool eastward displacement. Then abnormally warm conditions came back in 1993, a weak El Niño period which seemed to

be more characteristic of a slightly enhanced seasonal cycle [Boullanger and Menkes, 1995]. After a brief return of moderate conditions in late 1993 and the beginning of 1994, warm conditions returned during the last semester of 1994. This last semester of 1994 was characterized by a series of westerly wind bursts [Eldin *et al.*, 1997]. The modeled variability is in very good agreement with the data both in terms of dynamic height and warm pool eastward displacement. During this time period the eastward shift of the warm pool was particularly pronounced, followed by a retreat of the warm pool position to the dateline during the first semester of 1995. This corresponded to weak cold conditions in the Pacific [Goddard and Graham, 1997].

These east-west oscillations of the eastern edge of the warm pool can be attributed to zonal advection by eastward currents [Picaut *et al.*, 1996]. During the FLUPAC and OLIPAC cruises this resulted in positive SST anomalies as high as 2°C [NOAA, 1994] in the central Pacific in October–November 1994. Associated with the warm pool displacement and the series of westerly wind bursts, a series of downwelling Kelvin waves that may have further contributed to the eastward shift of the warm pool [Picaut and Delcroix, 1995] were generated in September, in November, and in December 1994 when the FLUPAC and OLIPAC cruises took place.

The first one was partly generated by a westerly burst near 160°E in early September [Eldin *et al.*, 1997]. Following the September wave, a westerly wind event occurred in October [Eldin *et al.*, 1997] at the beginning of the FLUPAC equatorial transect. This pulse, however, did not generate any clear propagation of Kelvin wave signal in neither the TAO dynamic height (Figure 2a), the TOPEX/POSEIDON sea level anomaly (not shown), nor the model (Figure 2b). At that time the zonal current observed by the TAO ADCP mooring located at 165°E indicates westward flow down to a 100 m depth. Hence the downwelling wave may have been damped by the interaction with the surrounding flow in opposite (westward) direction to the wave-induced eastward current [Brossier, 1987; McPhaden *et al.*, 1986]. Another reason may be that a reinforcement of easterlies in the central Pacific, at that time, counteracted the genesis of the downwelling Kelvin wave. Then, in November, a marked westerly wind burst generated a clear downwelling Kelvin wave that propagated across the basin. The OLIPAC passage at the equator occurred while the Kelvin wave associated sea level was rising. Lastly, a strong westerly burst at the beginning of December 1994 forced a strong downwelling Kelvin wave and is observed propagating all the way to the eastern Pacific. It marks the end of Kelvin wave activity in the western Pacific (Figure 2) and of the eastward shift of the 28°C isotherm.

Remotely forced processes such as the downwelling Kelvin waves have been thought to affect the geochemical (nutrients) and biological (chlorophyll, primary production, plankton community structure) fields [Murray *et al.*, 1994; Bidigare and Ondrusek, 1996]. They also contribute to the zonal displacement of the eastern edge of the warm pool. Thus the FLUPAC and OLIPAC cruises sampled the ocean during a period of time that appears to be affected by major features of the large scale equatorial dynamics which characterize the equatorial Pacific.

3.2. Vertical Physical and Biogeochemical Structures During FLUPAC and OLIPAC

3.2.1. Cruises data. The meridional FLUPAC transect at 165°E first sampled the tropical waters of the Coral Sea in the south and then entered the warm pool waters (SST > 28°C) at ~10°S (Figure 3a). During this transect, conditions were close to the reference conditions described in Radenac and Rodier [1996]. The thermocline was rather diffuse as opposed to the halocline (Figure 3b) which was well marked and shallower than the thermocline and decoupled from it. This decoupling was particularly apparent at 4°S–2°N where a low-salinity core (<34.1 practical salinity unit (psu)), associated with the westward flowing South Equatorial Current (SEC), was found from the surface down to 100 m depth. At ~150 m depth, south of the equator, the high-salinity core (>34.9 psu) was characteristic of South Pacific waters of subtropical origin. The Equatorial Undercurrent (EUC) was well developed with a maximum speed of 50 cm s⁻¹ at 175 m (Figure 3c). As is often observed at this longitude, the surface mixed layer was nitrate-exhausted all along this transect down to ~75 m, including the region close to the equator (Figure 3d). The nutricline closely followed the halocline, and the subsurface chlorophyll maximum (Figure 3e) that peaked at 0.5 µg L⁻¹ was found at the nutricline depth as is commonly observed.

During the OLIPAC cruise the isotherms near the equator at 150°W showed the characteristic spreading indicating the presence of the EUC core at 150 m depth (Figures 4a and 4c). They slowly and gradually spread and deepened to the south as was previously described during the Hawaii–Tahiti shuttle experiment [Wyrski and Kilonsky, 1984]. Around 150 m the high-salinity tongue originating from South Pacific subtropical waters (Figure 4b) penetrated from the south toward the equator. The core of the EUC had a maximum velocity of 70 cm s⁻¹ (Figure 4c). Above it the flow remained eastward almost up to the surface. Farther south, currents were weak and mostly westward except around 10°S where an eastward flow was measured, as is occasionally reported in the central Pacific [Eldin, 1983; Wyrski and Kilonsky, 1984; Kessler and Taft, 1987]. The observed distribution of nitrate (Figure 4d) was close to those previously described in the central Pacific [Carr *et al.*, 1992; Wyrski and Kilonsky, 1984; Murray *et al.*, 1995]. The mixed layer was nutrient depleted south of 10°S. To the north, surface concentrations were similar to the values observed during the 1992 spring EqPac cruise characteristic of El Niño warm conditions [Murray *et al.*, 1994]. Corresponding to this nitrate structure, the chlorophyll distribution showed a deep chlorophyll maximum below the top of the thermocline in the southern part of the section and showed relatively high chlorophyll values (>0.25 µg L⁻¹) extending from 100 m up to the surface to the north (Figure 4e). This transition from an oligotrophic regime to a mesotrophic one has been previously described in the area between 130° and 140°W, where its latitude varied between 10° and 14°S [Dandonneau and Eldin, 1987].

Both at depth and at the surface the equatorial FLUPAC transect sampled two different physical regimes which are more extensively described by Eldin *et al.* [1997]. The boundary between these two regimes is best evidenced in Figure 5b which shows a sharp salinity front of ~0.8 psu near

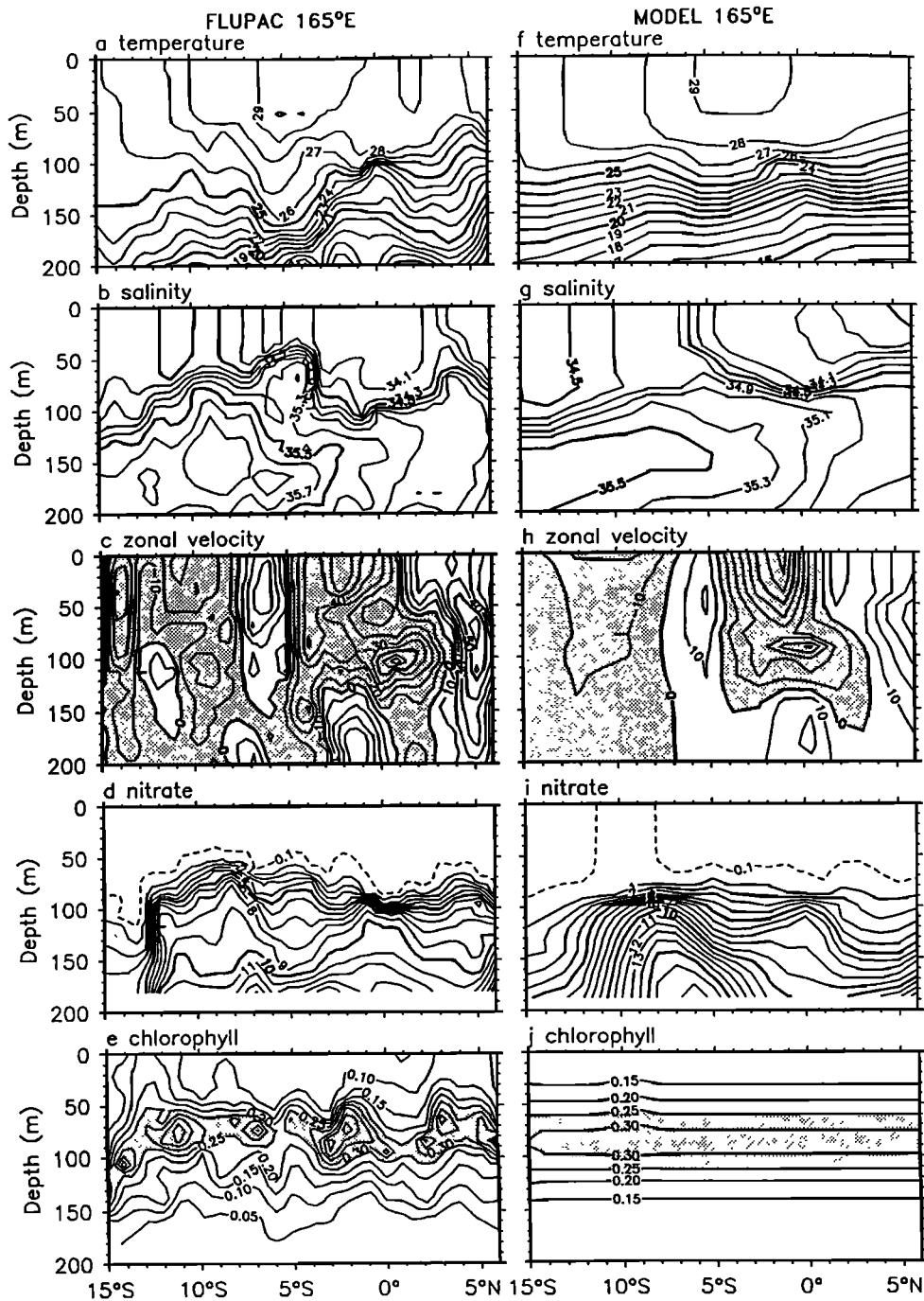


Figure 3. (a) Temperature ($^{\circ}\text{C}$), (b) salinity (practical salinity unit (psu)), (c) zonal velocity (cm s^{-1}), (d) nitrate ($\mu\text{mole kg}^{-1}$), and (e) chlorophyll ($\mu\text{g L}^{-1}$) observed during FLUPAC along 165°E and (f-j) simulated by the OPA-ERS-1 model. Westward currents are shaded.

175°W . The fresh (<35 psu) and warm ($29^{\circ}\text{--}30^{\circ}\text{C}$) waters west of this front were characteristic of the warm pool waters with a salinity barrier layer above the thermocline [Lukas and Lindstrom, 1991], representing the continuity at depth of the east-west surface front. A well-marked thermocline was located between 100 and 125 m all along this transect (Figure 5a), and the absence of an east-west slope was characteristic of El Niño conditions [Philander, 1989]. The surface current

(Figure 5c) showed a dominantly westward SEC except in the eastern part of the transect where the westward flowing SEC usually prevails [Wyrki and Kilonsky, 1984; Kessler and Taft, 1987; Eldin et al., 1997]. Nevertheless, surface current reversal has been commonly observed at this longitude, in springtime, during El Niño periods and/or associated with downwelling Kelvin waves [Firing et al., 1983; Kessler and McPhaden, 1995]. The patch of eastward current, observed

near 175°W, was probably associated with the October westerly wind event [Eldin *et al.*, 1997]. At subsurface a strong westward current was situated right above the thermocline in the west. This type of structure, already observed west of the salinity front, has been interpreted as the response to a westerly wind forcing [Kuroda and McPhaden, 1993]. It can also be indicative of the dynamics associated with subduction of the SEC under the salinity barrier layer as explained by Vialard and Delecluse [1998a, b]. The EUC was located beneath and tilted upward toward the east. The distribution of chlorophyll concentration was consistent with the salinity distribution (Figure 5e): the salinity front separated chlorophyll poor waters in the warm pool from

upwelling waters where chlorophyll was more abundant. At first sight this front similarly separated nitrate-exhausted water of the warm pool from the nutrient rich upwelling region (Figure 5d). However, one can note a spatial offset between nitrate-exhausted waters ($[\text{NO}_3] < 0.1 \mu\text{mole kg}^{-1}$) and the salinity or chlorophyll front ($[\text{Chl}] < 0.1 \mu\text{g L}^{-1}$) or zooplankton front (Figure 1). This offset was most probably controlled by biological processes in which nutrient removal by phytoplankton exhausted the nitrate dynamical supply near the barrier layer. The nitrate concentration increased eastward, reaching values $> 3 \mu\text{mole kg}^{-1}$ at 150°W. In the upwelled waters, consistent with the availability of nitrate in the upper well-lighted waters, the chlorophyll maximum was located in

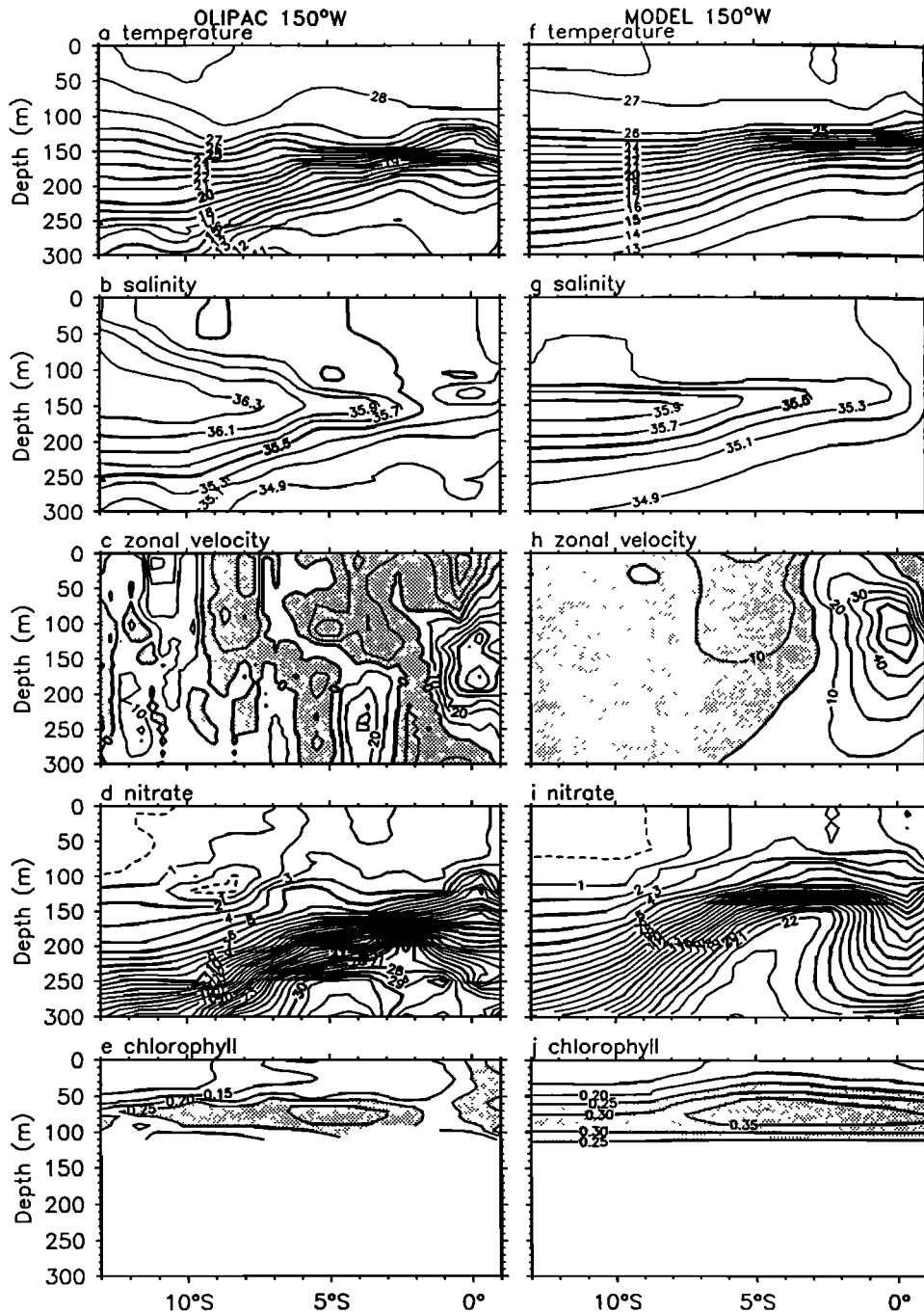


Figure 4. Same as Figure 3 but for the OLIPAC section along 150°W.

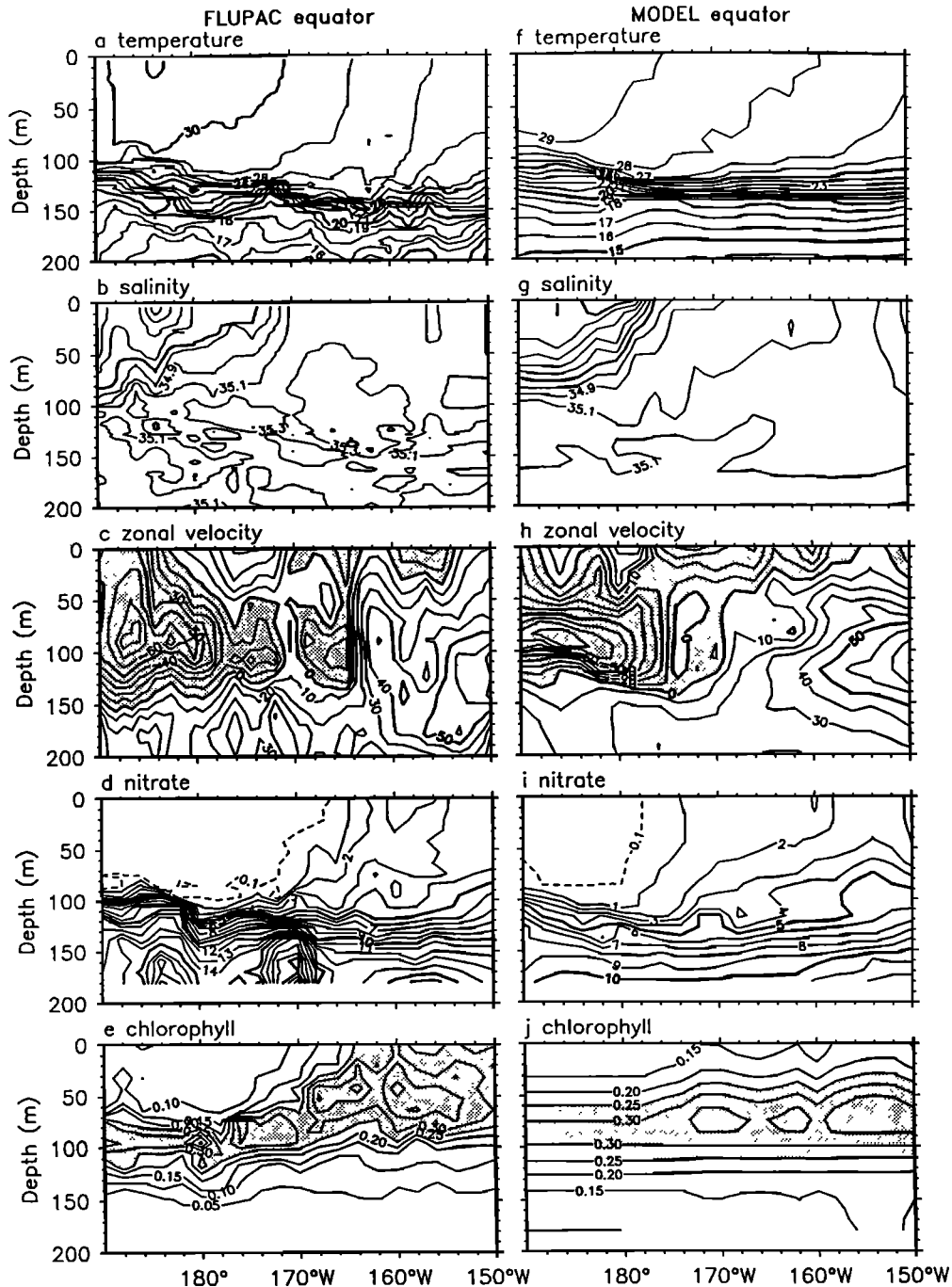


Figure 5. Same as Figure 3 but for the FLUPAC equatorial section.

the surface mixed layer. On the warm pool side a deep (80 m) chlorophyll maximum was positioned just below the salinity barrier layer at the top of the nutricline. The chlorophyll concentration in the deep maximum was $\sim 0.30 \mu\text{g L}^{-1}$ and was similar to that found in the upwelled waters farther east. In terms of biomass per square meter, however, the upwelled waters were richer than the warm pool waters because the chlorophyll rich layer was thicker there (see also section 4). Hence the FLUPAC equatorial data highlighted one of the most remarkable features of the equatorial Pacific: the warm, fresh, and oligotrophic waters of the western Pacific warm pool are separated by a sharp salinity front from the colder,

saltier, and mesotrophic waters of the upwelling waters. These two contrasted regimes are also evidenced in the upper trophic levels such as zooplankton distribution (Figure 1).

3.2.2. Model results. At 165°E , modeled temperatures are generally in good agreement with the data at the same depth (Figure 3f). However, the model temperature shows less spatial structure than the data, and in particular, it fails to reproduce the spreading of isotherms in the core of the EUC. The fresher water (<34.1 psu) in the equatorial region is correctly simulated although the surface front south of 4°S is more intense than in the observations (Figure 3g). The modeled EUC is much weaker than the observed (Figure 3h).

This discrepancy explains the lack of spreading of the isotherms in the modeled temperature. It has to be noted that the modeled current structures are much simpler than the observed and that countercurrents are generally too weak in this simulation.

At 150°W, thermohaline structures are generally well reproduced, but there are systematic biases such as colder temperatures in the upper layers and fresher waters in the salinity field. Zonal velocity shows patterns that are too smoothed (Figures 4c-4h) as compared to data and do not present any current variability south of 5°S. It has also to be stressed that the EUC core is too shallow.

In contrast, the equatorial transect is quite well simulated. The temperature distribution is good despite a 1°C bias in the upper layer waters (Figure 5f). The salinity field (Figure 5g) is well simulated. In particular, the salinity zonal gradient and its location are well reproduced. Being able to correctly simulate this gradient is crucial as it was seen to separate two different regimes. In the western part of the equatorial transect the EUC is weaker in the model than in the data and tilts upward toward the east where both data and model agree better (Figure 5h).

Considerations about dynamical simulations of these three particular transects are consistent with the more general conclusions of *Grima et al.* [1998]: the EUC core and the thermocline depth are shallower in the model than in the data, and the thermocline is generally too diffuse (as most modeled thermocline) and the countercurrents are too weak in the model.

In the oligotrophic region (warm pool), at 165°E, the surface NO₃ depletion (Figure 3i) is deeper than the observed and the nutricline tends to be too diffuse compared to observations. This can drive significant differences between observations and model outputs below the mixed layer. Reasons for this are certainly various. Among those the tendency of the model to have a too diffuse pycnocline structure can be invoked, as the nutricline is, at first order, shaped by the pycnocline structure in observations [*Radenac and Rodier*, 1996]. Discrepancies between the data and model due to limitations of the biological nitrate sink will be evoked later in the text.

At 150°W, the upper layer NO₃ concentrations are reasonable, and the transition between nutrient poor ($[\text{NO}_3] < 0.1 \mu\text{mole kg}^{-1}$) and nutrient rich waters is fairly well reproduced (Figure 4i). At depth, obvious biases show up such as a too shallow nutricline. It is hard to understand what factors control these biases in such complex 3-D dynamics. However, some of the spurious nutrient trapping near the surface may be related to the lack of horizontal transport of organic nitrogen as evoked in the model description [*Najjar et al.*, 1992; *Bacastow and Maier-Reimer*, 1991]. In the equatorial region the simulated nitracline shows a weaker than observed doming associated with the EUC core. This lack of structure is obviously related to the simulated EUC that is too shallow compared to the data (Figures 4c-4h).

Along the equator the surface transition between nutrient poor (oligotrophic) and nutrient rich (mesotrophic) waters is correctly simulated (Figure 5i). In the model this surface transition in the nitrate field is totally correlated to the salinity front at that period of time (see section 4). Therefore, if the offset seen in the data between the salinity front and nitrate-exhausted waters is indeed related to biological activity, our

simple nitrate sink model does not reproduce this process. At depth, however, this transition is found at the bottom of the barrier layer, as in the data, which indicates that processes maintaining the depth of the poor pool differ from those maintaining the barrier layer. Underneath the photic layer the nutricline is too diffuse compared to the data.

The chlorophyll values, which are statistically computed in the model, show higher surface concentrations and a much smoother pattern than are in the observations (Figures 3j, 4j, and 5j). This is not surprising as the statistics used here have been derived globally and thus cannot account for local variations as observed along the transect. The position and values of the deep maximum chlorophyll are rather well captured by the statistics. In the mesotrophic region, modeled chlorophyll is generally 30%-40% too high compared to observations but the deep chlorophyll maximum is well located (Figures 4j and 5j).

The validations of the coupled dynamical-biogeochemical conditions along the FLUPAC and OLIPAC transects have shown that despite imperfections the model is able to reproduce the major observed features at specific locations and times with good qualitative agreement. In particular, one important aspect and one merit of these simulations are that they are able to reproduce the two contrasted regimes of the equatorial waters.

4. The Modeled New Production

4.1. Modeled New Production at the Equator From 1992 to 1995

The variability of temperature and salinity distributions, currents, and dynamic topography of the model outputs is in good agreement with TAO buoy observations over 1992-1995 (see above and *Grima et al.*, [1998]), and the modeled nitrate field is also reasonable compared to the observations (see above). This allows us to investigate further the large-scale equatorial features of coupled conditions during 1992-1995 as given by the simulations. Figure 6 shows the equatorial section of modeled sea surface salinity (SSS), zonal currents, and new production. The succession of westward and eastward zonal currents is responsible for the zonal displacement of the eastern edge of the warm pool and fresh pool (SSS < 34.8 psu). The mechanisms creating these east-west migrations are detailed by *Picaut et al.* [1996] and by *Delcroix and Picaut* [1998]. Thus the warm/fresh/poor pool region is moved east and west according to the large-scale ENSO-related zonal current.

In this model output (Figure 6) the well-marked salinity front (Figure 6a) that separates the fresh warm pool to the west from the upwelling region moves eastward and westward and is displaced by the zonal currents (Figure 6b). Strong pulses of eastward velocities are shown to be associated with the occurrences of downwelling Kelvin waves such as those of November-December 1992 and 1994. The SSS front is seen to be particularly pronounced during these events when current convergence at the front is particularly strong. The last semester of 1994 is the longest period when the zonal current is mostly eastward. This causes the front and the eastern edge of the warm pool (position of the 28°C isotherm) to gradually move eastward and to sharpen. When eastward currents are not so strong or westward currents occur, the salinity front is

more diffuse (Figures 6a and 6b) [Vialard and Delecluse, 1998a, b].

Primary production allows us to differentiate between the equatorial poor and rich regimes (Figure 6c). Figure 6c clearly shows that during the 1992-1995 period, two distinct regimes prevailed that are characteristic of the warm pool (poor pool) region on one side and the upwelling region where waters are richer on the other side. These two regimes are separated by a "primary production front" that is closely related to the salinity front (see the position of the 34.8 psu isohaline and the primary production front on Figure 6c). Only during the first three months of the simulation, a decoupling between the new production and salinity front occurs. This time period should be considered with caution in the simulation as it is close to the ending of the 5 year spin up calculated with a perpetual April 1992 to March 1993 year. Note that the relation between the primary production front and the eastern edge of the warm pool is particularly strong when the salinity front is well marked, in November-December 1992 and during the last semester of 1994, and closely follows the displacements of the salinity front. The FLUPAC and OLIPAC cruises sampled this last episode.

As seen in Figure 5, observed nitrates at the time of FLUPAC closely reflect the position of the simulated primary production (nitrate) front which is therefore displaced via zonal advection during the period of interest. Additional data from November-December 1994 [Inoue *et al.*, 1996] show that the modeled front position is also in agreement with observations at that time. The variables recorded along the

equator during FLUPAC further confirm that the front actually separates the oligotrophic warm pool region from a mesotrophic regime east of the front (Figure 1). Consequently, primary production can vary greatly during El Niño or La Niña periods because of these large east-west displacement patterns of the warm pool. For example, it was greatly reduced during late spring of 1992, at 140°W, in agreement with the observations made during the EqPac spring cruises [Murray *et al.*, 1995]. However, further simulations of the ENSO cycle are required to really estimate primary production reduction when strong El Niño occurs. In particular, spectacular impacts of the 1997-1998 El Niño should give further insights on such reductions.

4.2. Comparison Between the Warm Pool and the Upwelling Regimes

Given the clear separation between the regimes, it is useful to introduce the NINO4 (160°E-150°W, 5°S-5°N) and NINO3 (150°-90°W, 5°S-5°N) boxes often used to contrast two dynamical (warm pool and upwelling) regions for ENSO-related issues [NOAA, 1994]. Indeed, during the 1992-1995 time period one can see that these two regions correspond to the warm pool region (NINO4) and the upwelling region (NINO3). Averaged primary production amounts to ~ 0.9 mmol NO₃ m⁻² d⁻¹ in NINO4 and 2.1 mmol NO₃ m⁻² d⁻¹ in NINO3. These can be thought of as representative of mean conditions during this weak ENSO period for the two regimes.

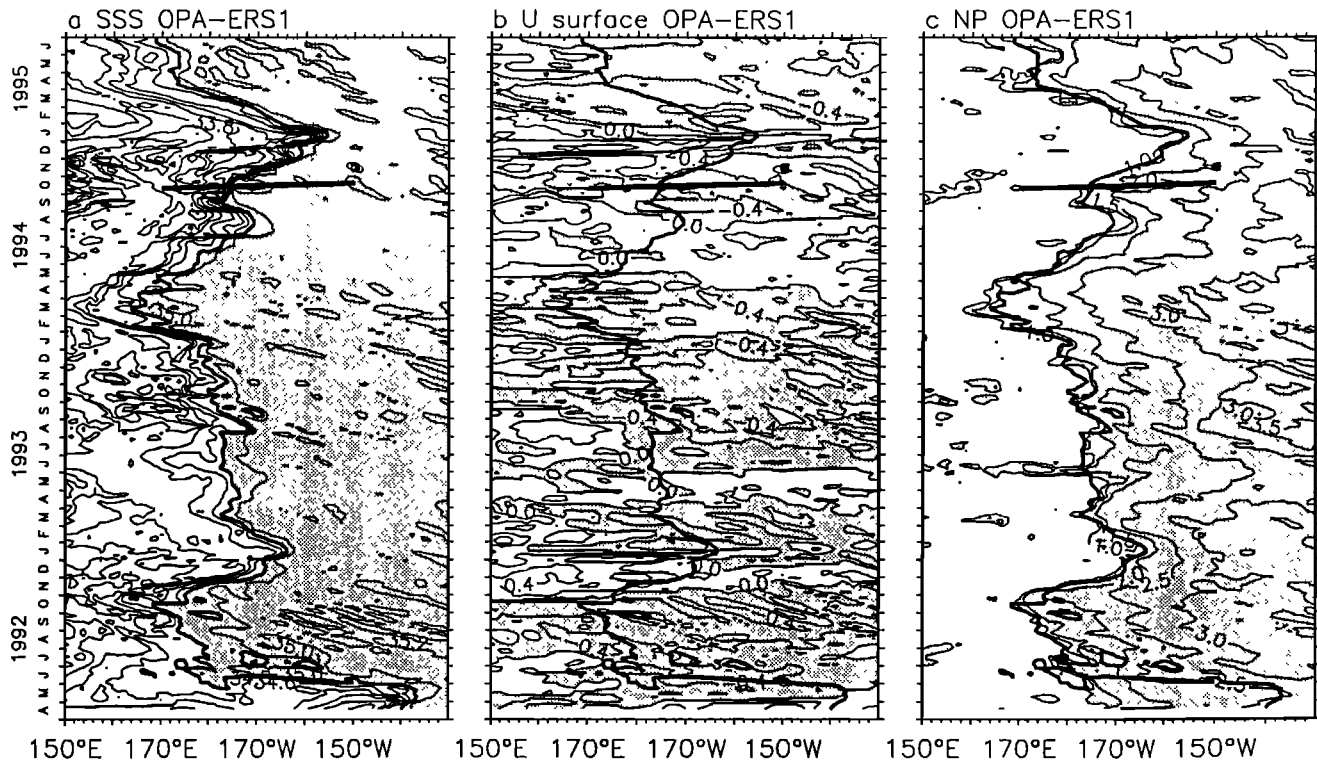


Figure 6. OPA-ERS-1 model outputs along the equator for the whole simulation: (a) salinity (psu), (b) zonal velocity component (cm s^{-1}), (c) new production ($\text{mmol NO}_3 \text{ m}^{-2} \text{ d}^{-1}$). Sea Surface Salinity (SSS) > 34.8 psu, westward currents, and new production > 1 $\text{mmol NO}_3 \text{ m}^{-2} \text{ d}^{-1}$ are shaded. The 34.8 psu isohaline marking the SSS front is superimposed on Figures 6a-6c. The FLUPAC equatorial transect is superimposed as a dark line in September-October 1994, and the OLIPAC cruise is represented by a dot at 150°W in November 1994.

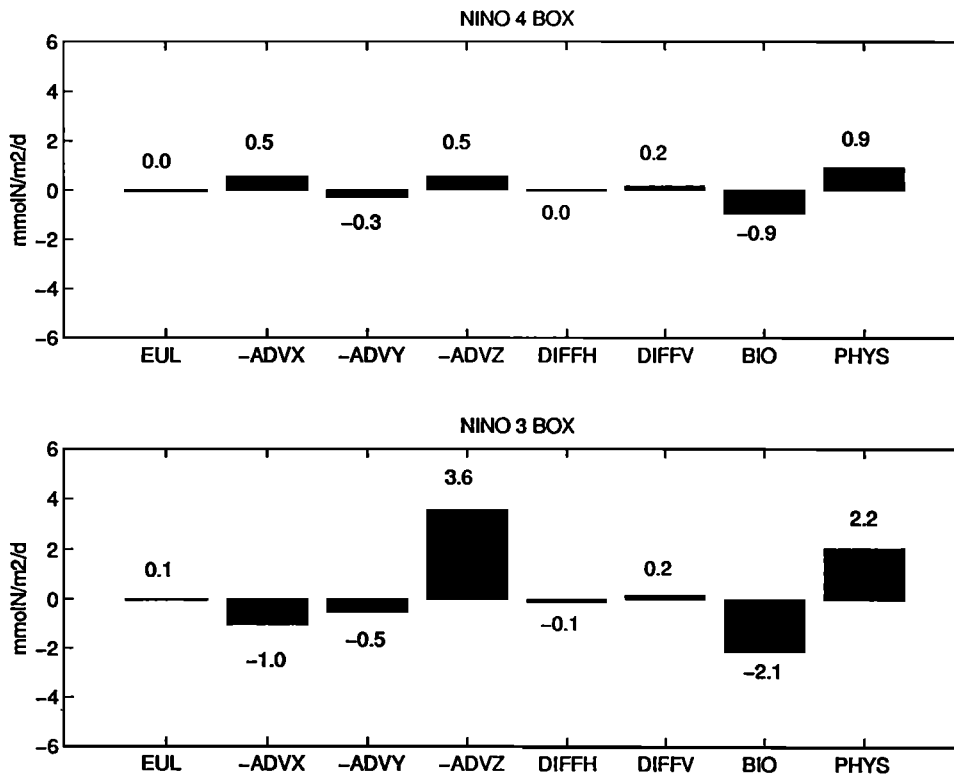


Figure 7. Budgets of nitrate terms of (1) integrated from the surface down to the euphotic layer depth in the NINO3 and NINO4 boxes for the 1992-1995 simulation. -ADVX, -ADVY, -ADVZ are the zonal, meridional and vertical advection terms; DIFFH and DIFFV are the contributions of horizontal and vertical diffusion terms; BIO is the nitrate sink (new production) and $PHYS = -(ADVX + ADVY + ADVZ) + DIFFH + DIFFV$. The eulerian term $EUL = PHYS + BIO$

So far, model simulations are the only way to seize the large-scale primary production variations as shown above. The model further allows us to understand the dynamics underlying the regimes that are observed. We have stressed the contrast between the warm/fresh/poor and cold/salty/rich equatorial regimes, and we can now estimate the budgets that lead to these two contrasted regimes. Budgets of nitrate integrated from the surface down to the euphotic layer depth are calculated in the NINO4 and NINO3 boxes by integrating (1) over the photic layer. This gives a representation of the respective roles of biology and the dynamics for the control of nitrate of the photic layer.

Figure 7 shows the relative contribution of all terms in the vertical integration of (1) for NINO4 and NINO3 boxes. The last histogram bar sums up the contribution of all the advective and diffusive terms and thus represents the physical forcing. In each case, eulerian terms are nearly zero so that one can understand the distribution of nitrate as a sum of dynamical effects and biological uptake. In the warm and poor pool region (NINO4), the supply of nitrate is mainly due to horizontal advection by the SEC (not shown here) that brings nitrate richer waters from NINO3 region and to upwelling of richer waters from beneath the photic layer, which in that region roughly corresponds to the nitracline depth. Some losses are conveyed by meridional divergence. This all amounts to a new primary production that is ~ 0.9 mmol NO_3 , $m^{-2} d^{-1}$. As expected, the NINO3 region is much more dynamical, and production is much higher. Contrary to NINO4, the dominant physical forcing is vertical advection of

richer waters from the EUC core (not shown here) which confirms the results given by *Chai et al.* [1996] at $0^\circ, 140^\circ W$. This upwelling of the nitrate effect is somewhat counterbalanced by meridional divergence and loss of nitrate to the west by horizontal advection. This analysis illustrates the variety of processes that control nitrate concentrations and shows that the coupling between biology and physics can only be envisioned in a 3-D way.

4.3. Comparison With Other Results

At this point it is worth saying that our simple biological sink with constant V_{max} and K_{NO_3} parameters is able to reproduce the major features of such two different regimes as the warm pool and upwelling regimes. The simplicity of the biogeochemical model adopted in this work is based on the empirical nitrate-chlorophyll linear relationship. In earlier versions of the model in which the nitrate sink was computed without chlorophyll it proved impossible to correctly reproduce the nitrate field observed during FLUPAC and OLIPAC. It must, however, be recognized that there is no objective reason why the nitrate-chlorophyll relationship at the surface should be linear. The correlation between these two variables is low. The lack of correlation partly arises from the chlorophyll measurements that are affected by a relatively important instrumental error (filtration, pigments extraction, acidification step, etc.) and by short-term variability. Modern data are rare, and ancient data suffer from intercalibration problems. This dispersion prevents us from finding out in the

data a more comprehensive nitrate-chlorophyll relationship. The assumption that chlorophyll at the surface is linearly and positively related to nitrate is certainly not valid everywhere in the equatorial Pacific. For instance, in the eastern Pacific the surface waters with high NO_3 (and Fe) content brought up to the surface by the upwelling have a low chlorophyll content at the source of the upwelling, which then grows up very quickly while NO_3 decreases. Nevertheless, most of the equatorial Pacific is occupied by phytoplankton populations dominated by the picoplankton [Blanchot *et al.*, 1992] and seems to respond to the environment like an oligotrophic ecosystem, whatever the nutrient-exhausted waters or the HNLC waters are considered [Landry *et al.*, 1997]. This relative uniformity of the equatorial Pacific makes it reasonable to use a single relationship to estimate the chlorophyll at the surface using nitrate concentration, and the existing information only permits us to use a linear relationship. It has also been noted that the statistical and the observed chlorophyll fields were not in agreement in some parts of the studied domain. The effect of these discrepancies on the adjusted nitrate sink caused by photosynthesis should be small because the bias itself is relatively small and because it occurs at depths where only 1%-10 % of incident light penetrates, so that the error on integrated new primary production is only a few percent. Thus, in spite of many subtleties that the simple model obviously cannot account for, the biological sink, as modeled, allows us to investigate the new production in the photic layer of the warm pool and of the upwelled waters.

The V_{max} and K_{NO_3} values which give the best fit with the FLUPAC and OLIPAC observations of nitrate concentration are $4 \times 10^{-3} \mu\text{mol NO}_3, \text{mg Chl}^{-1} \text{s}^{-1}$ and $0.01 \mu\text{mol NO}_3, \text{kg}^{-1}$, respectively. These values are not directly comparable to observations made during FLUPAC and OLIPAC, where only the in situ incorporation of $^{15}\text{NO}_3$ at ambient NO_3 concentration was measured and not the kinetics of NO_3 assimilation. It is possible, however, to compare the biological sink of nitrate, i.e., new production, computed by the model to the NO_3 assimilation measured during the cruises and integrated over the photic layer. The nitrate taken up by photosynthesis in the model at the equator from 1992 to 1995 is shown on Figure 6. The values integrated from the surface to the bottom of the photic layer are $<1 \text{ mmol NO}_3, \text{m}^{-2} \text{d}^{-1}$ in the oligotrophic warm pool and between 2 and $3 \text{ mmol NO}_3, \text{m}^{-2} \text{d}^{-1}$ at $0^\circ, 150^\circ\text{W}$ in the nitrate rich, upwelled waters east of the salinity/nitrate/chlorophyll front.

The measurements using $^{15}\text{NO}_3$ made during FLUPAC at $0^\circ, 167^\circ\text{E}$ (oligotrophic warm pool) show that nitrate fixation was $\sim 1 \mu\text{mol NO}_3, \text{m}^{-3} \text{h}^{-1}$ from the surface to 100 m depth, which represents $\sim 1.2 \text{ mmol NO}_3, \text{m}^{-2} \text{d}^{-1}$ for a 12 or 24 hour

period. (McCarthy *et al.* [1996] indeed observed that most of the nitrate assimilation occurs during the daylight period.) During OLIPAC along 150°W the average of nitrate assimilation measurements made south of 10°S (oligotrophic south Pacific subtropical gyre), both along the transect and during the fixed station at 16°S , was $0.74 \text{ mmol NO}_3, \text{m}^{-2} \text{d}^{-1}$ [Moutin and Coste, 1996], very similar to the average determined from the warm pool while under a different regime (less sharp pycnocline and weaker vertical shear of current). The $^{15}\text{NO}_3$ uptake experiments made during the EqPac cruises at latitudes $>6^\circ$ (off the equatorial upwelled waters) range between 0.2 and $1 \text{ mmol NO}_3, \text{m}^{-2} \text{d}^{-1}$ [McCarthy *et al.*, 1996]. Considering that the diffusion of colder, nitrate rich water through the 26°C isotherm should equilibrate the heat flux from the atmosphere into the ocean, in the domain defined by SST $> 26^\circ\text{C}$ (i.e., the warm pool), Peña *et al.* [1994] estimated that new production in this domain was on average $15 \text{ g C m}^{-2} \text{y}^{-1}$. Assuming that nitrate and carbon assimilation follows the C:N = 6.6 Redfield ratio, this amounts to a new production equal to $0.52 \text{ mmol NO}_3, \text{m}^{-2} \text{d}^{-1}$ which is in rather good agreement with the above measurements and with the values given by our model.

In the nitrate rich upwelled waters at $0^\circ, 150^\circ\text{W}$, nitrate fixation measured during FLUPAC in late October amounted to $3 \text{ mmol NO}_3, \text{m}^{-2} \text{d}^{-1}$, a value greater than that obtained at $5^\circ\text{S}, 150^\circ\text{W}$ during OLIPAC in November: $1.4 \text{ mmol NO}_3, \text{m}^{-2} \text{d}^{-1}$ [Moutin and Coste, 1996]. The decrease in the nitrate concentration between the two cruises, consecutive to the strengthening of El Niño conditions, is an explanation for this relatively low value. The front between the warm pool and the upwelled waters indeed shifted rapidly to the east in October and November 1994 (Figure 6), inducing a rapid decrease of new production at 150°W . During the EqPac cruises, nitrate fixation was more intense at the equator (2°N - 2°S) than at higher latitudes and averaged to $0.7 \text{ mmol NO}_3, \text{m}^{-2} \text{d}^{-1}$ during the spring cruise, dominated by El Niño conditions, versus $2.8 \text{ mmol NO}_3, \text{m}^{-2} \text{d}^{-1}$ in the autumn, when upwelling conditions re-established [McCarthy *et al.*, 1996]. These fall values are in agreement with the model results (Figure 6), but the model overestimates new production during the spring cruise. However, modeled new production at that time should be taken with care as is previously explained in paragraph 4.1. Thus, in the model the nitrate fixation integrated over the photic layer which generates a nitrate field that fits best with that observed during FLUPAC and OLIPAC is in agreement with the measurements made during FLUPAC and OLIPAC using ^{15}N experiments and during the EqPac fall cruise.

Large-scale estimates made for the 90° - 180°W , 5°N - 5°S domain are listed in Table 1. Chavez and Barber [1987]

Table 1. Estimates of New Production in the Equatorial Pacific Upwelling Region: 90°W - 180° , 5°N - 5°S

Origin	Estimate $\text{mmol NO}_3, \text{m}^{-2} \text{d}^{-1}$
Chavez and Barber [1987] using primary production and an f ratio of 0.44	2.7
F. Chai <i>et al.</i> [1996] using ecosystem model in the upper 120 m	2.3
Ku <i>et al.</i> [1995] using the ^{228}Ra budget in the euphotic zone (EqPac)	2.5
Toggweiler and Carlson [1995] using an ecosystem model	3.3
This study during 1992-1995 using the model	2.3

estimated that the 5°S-5°N zone, east of the dateline (i.e., the "equatorial cold tongue" [Wyrki, 1981]), could support a yearly new production of 0.8 gigatons of carbon during normal conditions, which represents 2.7 mmol NO₃ m⁻² d⁻¹. *Ku et al.* [1995] estimated a new production of 2.5 mmol NO₃ m⁻² d⁻¹ during the 1992 El Niño period. New production in the equatorial Pacific has also been estimated by 3-D coupled physical-biogeochemical models. Using average seasonal winds and heat forcings, *Toggweiler and Carson* [1995] found that the average new production in the 5°N-5°S, 90°-180°W area is 41.9 10⁴ mol NO₃ s⁻¹, i.e., 3.3 mmol NO₃ m⁻² d⁻¹. A similar model estimate by *Chai et al.* [1996], using an average seasonal forcing, amounts to 2.3 mmol NO₃ m⁻² d⁻¹. Another 2-D modeling approach by *Carr et al.* [1995], based on the physical observations during the Wecoma cruise in 1988 (La Niña conditions), leads to an estimate of 4.4 mmol NO₃ m⁻² d⁻¹ in the central equatorial Pacific. Our estimation of new production in the same region is 2.3 mmol NO₃ m⁻² d⁻¹. Considering that the 1992-1995 period was affected by warm conditions, our estimation of 2.3 mmol NO₃ m⁻² d⁻¹ should be considered as representative of El Niño conditions.

Such low values imply that the residence time of nitrate in the surface mixed layer is very long. Dividing the nitrate content of the mixed layer by the daily nitrate assimilation rate, *McCarthy et al.* [1996] found that the time required to deplete the mixed layer was of the order of 300 days. This long residence time is certainly a consequence of overall iron limitation in the region [*Martin, 1990; Barber, 1992; Price et al., 1994*]. The same computation here (based on the nitrate content of the euphotic zone during FLUPAC at 0°, 150°W, i.e., 300 mmol m⁻², and new production in the model, equal to ~2.3 mmol m⁻² d⁻¹) gives a residence time of the order of 130 days. In fact, the residence time should be even longer in our model because nitrate assimilation in the photic layer decreases the nitrate concentration at the surface, hence decreasing the prognostic chlorophyll at the sea surface and the vertical profile of chlorophyll in the photic layer computed according to *Morel and Berthon* [1989] and finally reducing new production. One can reasonably assume that the evolution of the mixed layer at sea follows a similar scheme. In addition, this crude computation ignores the vertical diffusion of nutrients through the pycnocline, which slowly but permanently refuels the mixed layer. Timescales to consume all the nitrate in the surface mixed layer of the equatorial Pacific should thus be of the order of 150-200 days, or even more, and this long duration is to be considered when examining the consequences of El Niño events on the primary production in the region: once El Niño conditions have settled, the nutrients upwelled during the previous La Niña episode can still fuel the new production of the equatorial Pacific for several months.

5. Conclusion

The equatorial Pacific presents two contrasted dynamical regimes: warm and fresh waters of the warm pool separated by a salinity front from the colder and saltier waters of the upwelling region. In this paper we have coupled the OPA-LODYC OGCM forced by ERS-1 winds to a nitrate transport model with a simple biological sink to estimate new production on large temporal and basin scales during the

1992-1995 weak El Niño. During the 1994 weak warm event the FLUPAC and OLIPAC French JGOFS cruises took place in the central and western equatorial Pacific.

These cruises sampled the equatorial Pacific when the warm pool was displaced eastward to ~160°W. This shift was characterized by the in-phase displacement of a salinity, nitrate, and chlorophyll front which separated two contrasted regimes: the oligotrophic warm pool waters to the west from the nitrate rich mesotrophic waters to the east. Consequently, the biomass observed, in terms of chlorophyll concentration, as well as the nitrate concentration in the photic layer to the east of this front were abnormally low, and biological fluxes were smaller than those observed on other cruises.

The best fit between modeled and observed nitrates gives a maximum speed of nitrate assimilation equal to 4 10⁻³ μmol NO₃ mg Chl⁻¹ s⁻¹ and a very low semisaturation constant (0.01 μmol NO₃ kg⁻¹) for the Michaelis-Menten function used in the sink. Given this and owing to a good agreement between the observed and modeled physical parameters, the coupled model reproduces a nitrate field for this period that is in rather good agreement with the nitrate concentrations measured both in the oligotrophic warm pool and the upwelling water. In particular, it is successful in simulating the transition between the two regimes. This allows us to place the FLUPAC and OLIPAC cruises into a larger-scale context and to examine the coupled physical-new production features of the 1992-1995 years with confidence.

During the 1992-1995 period the warm pool is shown to be associated with new production lower than 1 mmol NO₃ m⁻² d⁻¹ on average. This poor pool is separated from the richer waters of the upwelling (new production of ~2.3 mmol NO₃ m⁻² d⁻¹ in *Wyrki's* [1981] box) by a sharp new production front that is closely related to the sharp simulated salinity front. Such new production values agree with previous observational estimates. Such low values in the upwelling region can be considered as representative of weak El Niño conditions.

The salinity front at the eastern edge of the warm pool is subject to large zonal displacement in relation to ENSO-related zonal currents. Similarly, the transition between poor and rich waters experiences such huge zonal displacements due to zonal advection processes. In particular, when these fronts are displaced eastward in relation to El Niño eastward currents, new production can experience dramatic decreases. During the FLUPAC and OLIPAC cruises, new production was indeed low which can mainly be attributed to this eastward displacement of the poor pool. New production was also weaker than that measured 2 years earlier during the EqPac fall cruises along 140°W, during non-El Niño conditions, when the poor pool is shown to have retreated back.

This model has obvious flaws that reside in the oversimplification of the biological component. For instance, it was shown that nutrient trapping occurred in the east at depth. One way to improve that bias is to add a compartment of dissolved organic nitrogen in order to account for the horizontal transport of new production [*Stoens et al., 1998*] rather than instantaneously remineralizing the whole production into particulate matter [*Najjar et al., 1992*].

However, this model is a powerful tool for exploring the consequences of the strong coupling of the equatorial dynamics with biogeochemistry and biology of higher trophic

levels on seasonal to interannual time scales. For instance, other simulations are underway in order to reproduce strong El Niño and La Niña situations. So far, La Niña-related biological implications have been rarely observed [Radenac and Rodier, 1996] and will be assessed within the model context. Moreover, Figure 1 has shown that at the FLUPAC time the transition between the two regimes also corresponded to a sharp transition in CO₂ outgasing. Study is underway to couple this nitrate model to a carbon model in order to assess the global budgets and mechanisms of CO₂ fluxes to the atmosphere that are at work in the two contrasted warm pool and upwelling regimes. Such models with a simple physical-biogeochemical coupling have already proved successful in simulating the major nitrate trends and patterns as well as the major CO₂ fluxes in the equatorial Atlantic Ocean [Thomas, 1995; Loukos, 1995]. Finally, our modeled new production can be used in successfully simulating the position of tuna forage in the western Pacific [Lehodey et al., 1998] which experiences large east-west migrations in relation to ENSO [Lehodey et al., 1997].

Acknowledgments. The FLUPAC and OLIPAC cruises were a contribution to the JGOFS international study of the equatorial Pacific and were coordinated by JGOFS-France. Financial support was given by Institut Français pour l'Exploitation de la MER (IFREMER), by Institut National des Sciences de l'Univers (INSU) and by Institut Français de Recherche pour le Développement en Coopération (ORSTOM). Ship time was ensured by GENAVIR/IFREMER. We are grateful to the captain and crew of R/V l'Atalante for generous and efficient help during the cruise. We are also grateful to C. Bournot, J.-Y. Panche, and F. Gallois, who took care of the equipment and ensured the high quality of the CTD data. M. Rodier, S. Bonnet, and P. Gérard made the measurements of nutrients, and the chlorophyll measurements presented here have been made by P. Conan and by A. Le Bouteiller. Comments from A. Le Bouteiller and R. Le Borgne are greatly appreciated. We are indebted to M. McPhaden for fruitful comments. Finally, we thank both reviewers whose comments greatly improved our first manuscript.

References

- Bacastow, R., and E. Maier-Reimer, Dissolved organic carbon in modelling new production, *Global Biogeochem. Cycles*, 5: 71-85, 1991.
- Barber, R. T., Introduction to the WEC88 cruise: An investigation into why the equator is not greener, *J. Geophys. Res.*, 97, 609-610, 1992.
- Barber, R. T., and F. P. Chavez, Biological consequences of El Niño, *Science*, 222, 1203-1210, 1983.
- Bentamy, A., Y. Quilfen, N. Grima, F. Gohin, M. Lenaour, and J. Servain, Determinations and validation of average wind fields from ERS-1 scatterometer measurements, *Global Atmos. Ocean Syst.*, 4, 1-29, 1996.
- Bidigare, R. R., and M. E. Ondrusek, Spatial and temporal variability of phytoplankton pigment distributions in the central equatorial Pacific Ocean, *Deep Sea Res., Part II*, 43, 809-833, 1996.
- Blanchot, J., M. Rodier, and A. Le Bouteiller, Effect of El Niño Southern Oscillation events on the distribution and abundance of phytoplankton in the western Pacific tropical ocean along 165°E, *J. Plankton Res.*, 14, 137-156, 1992.
- Blanke, B., and P. Delecluse, Variability of the tropical Atlantic Ocean simulated by a general circulation model with two different mixed layer physics, *J. Phys. Oceanogr.*, 23, 1363-1388, 1993.
- Boulanger, P., and C. Menkes, Propagation and reflection of long equatorial waves in the Pacific Ocean during the 92-93 El Niño, *J. Geophys. Res.*, 100, 25,041-25,059, 1995.
- Brossier, F., Numerical modelling of equatorial waves in the presence of a mean current, *J. Phys. Oceanogr.*, 17, 1100-1113, 1987.
- Busalacchi, A. J., M. J. McPhaden, and J. Picaut, Variability in equatorial Pacific sea surface topography during the verification phase of the TOPEX/POSEIDON mission, *J. Geophys. Res.*, 99, 24,725-24,738, 1994.
- Carr, M.-E., N. S. Oakey, B. Jones, and M. R. Lewis, Hydrographic patterns and vertical mixing in the equatorial Pacific along 150°W, *J. Geophys. Res.*, 97, 611-626, 1992.
- Carr, M.-E., M. R. Lewis, and D. Kelley, A physical estimate of new production in the equatorial Pacific along 150°W, *Limnol. Oceanogr.*, 40, 138-147, 1995.
- Chai, F., S. T. Lindley, and R. T. Barber, Origin and maintenance of a high nitrate condition in the equatorial Pacific, *Deep Sea Res., Part II*, 43, 1031-1064, 1996.
- Chavez, F. P., and R. T. Barber, An estimate of new production in the equatorial Pacific, *Deep Sea Res., Part A*, 34, 1229-1243, 1987.
- Chavez, F. P., S. K. Service, and S. E. Buttrely, Temperature-nitrate relationships in the central and eastern equatorial Pacific, *J. Geophys. Res.*, 101, 20,553-20,563, 1996.
- Dandonneau, Y., Monitoring the sea surface chlorophyll concentration in the tropical Pacific: Consequences of the 1982-83 El Niño, *Fish. Bull.*, 84, 687-695, 1986.
- Dandonneau, Y., Surface chlorophyll concentration in the Tropical Pacific Ocean: An analysis of data collected by merchant ships from 1978 to 1989, *J. Geophys. Res.*, 97, 3581-3591, 1992.
- Dandonneau, Y., Sea-surface partial pressure of carbon dioxide in the eastern equatorial Pacific (August 1991 to October 1992): A multivariate analysis of physical and biological factors, *Deep Sea Res., Part II*, 42, 349-364, 1995.
- Dandonneau, Y., and G. Eldin, Southwestward extent of chlorophyll-enriched waters from the Peruvian and equatorial upwellings between Tahiti and Panama, *Mar. Ecol. Prog. Ser.*, 38, 283-294, 1987.
- Delcroix, T., and J. Picaut, Zonal displacement of western equatorial Pacific fresh pool, *J. Geophys. Res.*, 103, 1087-1098, 1998.
- Dequé, M., C. Dreverton, A. Braun, and D. Cariolle, The ARPEGE/IFS atmosphere model: a contribution to the French community climate modelling, *Clim. Dyn.*, 10, 249-266, 1994.
- Dugdale, R. C., and J. J. Goering, uptake of new and regenerated forms of nitrogen in primary productivity, *Limnol. Oceanogr.*, 12, 196-206, 1967.
- Eldin, G., Eastward flows of the south equatorial central Pacific, *J. Phys. Oceanogr.*, 13, 1461-1467, 1983.
- Eldin, G., M. Rodier, and M.-H. Radenac, Physical and nutrient variability in the upper equatorial Pacific associated with westerly wind forcing and wave activity, *Deep Sea Res., Part II*, 44, 1783-1800, 1997.
- Feely, R. A., R. Wanninkhof, C. E. Cosca, P. P. Murphy, M. F. Lamb, and M. D. Steckley, CO₂ distributions in the equatorial Pacific during the 1991-1992 ENSO event, *Deep Sea Res., Part II*, 42, 365-386, 1995.
- Firing, E., R. Lukas, J. Sadler, and K. Wyrтки, Equatorial undercurrent disappears during 1982-83 El Niño, *Science*, 222, 1121-1123, 1983.
- Goddard, L., and N. E. Graham, El Niño in the 1990s, *J. Geophys. Res.*, 102, 10,423-10,436, 1997.
- Grima, N., A. Bentamy, P. Delecluse, K. Katsaros, C. Levy, and Y. Quilfen, Sensitivity study of an OGCM to satellite wind-stress forcing, *J. Geophys. Res.*, in press, 1998.
- Hayes, S. P., L. J. Mangum, J. Picaut, A. Sumi, and K. Takeuchi, TOGA/TAO: A moored array for real-time measurements in the tropical Pacific Ocean, *Bull. Am. Meteorol. Soc.*, 72, 339-347, 1991.
- Herbland, A., A. Le Bouteiller, and P. Raimbault, Size structure of phytoplankton biomass in the equatorial Atlantic Ocean, *Deep Sea Res., Part A*, 32, 819-836, 1985.
- Honjo, S., Sedimentation of material in the Sargasso Sea at 5,367 m, *J. Mar. Res.*, 36, 469-492, 1978.
- Inoue, H. Y., M. Ishii, H. Matsueda, and M. Ahoyama, Changes in longitudinal distribution of the partial pressure of CO₂ (pCO₂) in the central and western equatorial Pacific, west of 160°W, *Geophys. Res. Lett.*, 23, 1781-1784, 1996.
- Kessler, W. S., and M. J. McPhaden, The 1991-1993 El Niño in the central Pacific, *Deep Sea Res., Part II*, 42, 295-333, 1995.

- Kessler, W. S., and B. A. Taft, Dynamic heights and zonal geostrophic transports in the central tropical Pacific during 1979-84, *J. Phys. Oceanogr.*, **17**, 97-122, 1987.
- Kiefer, D. A., and B. G. Mitchell, A simple, steady state description of phytoplankton growth based on absorption cross section and quantum efficiency, *Limnol. Oceanogr.*, **28**, 770-776, 1983.
- Ku, T., L. S. Luo, M. Kusakabe, and J. K. B. Bishop, ^{226}Ra derived nutrient budgets in the upper equatorial Pacific and the role of "new" silicate in limiting productivity, *Deep Sea Res., Part II*, **42**, 295-333, 1995.
- Kuroda, Y., and M. J. McPhaden, Variability in the western equatorial Pacific Ocean during Japanese Pacific climate study cruises in 1989 and 1990, *J. Geophys. Res.*, **98**, 4747-4759, 1993.
- Landry, M. R., et al., Iron and grazing constraints on primary production in the central equatorial Pacific: An EqPac synthesis, *Limnol. Oceanogr.*, **42**, 405-418, 1997.
- Le Borgne, R., and M. Rodier, Net zooplankton and the biological pump: A comparison between the oligotrophic and mesotrophic equatorial Pacific, *Deep Sea Res., Part II*, **44**, 2003-2023, 1997.
- Lehodey, P., M. Bertignac, J. Hampton, A. Lewis, and J. Picaut, El Niño-Southern Oscillation and tuna in the western Pacific, *Nature*, **389**, 715-718, 1997.
- Lehodey, P., J.-M. André, M. Bertignac, J. Hampton, A. Stoens, C. Menkes, L. Mémery, and N. Grima, Predicting skipjack tuna forage distributions in the equatorial Pacific using a coupled dynamical bio-geochemical model, *Fish. Oceanogr.*, in press, 1998.
- Levy, M., Modélisation des processus biogéochimiques en Méditerranée Nord-Occidentale: Cycle saisonnier et variabilité mésoéchelle, Ph.D. dissertation, 331 pp., Univ. de Paris VI, Paris, 1996.
- Loukos, H., Simulation du cycle océanique du carbone dans l'Atlantique équatorial. Validation de l'année 1983 (FOCAL), Ph.D. dissertation, 207 pp., Univ. de Paris VI, Paris, 1995.
- Lukas, R., and E. Lindstrom, The mixed layer of the western equatorial Pacific Ocean, *J. Geophys. Res.*, **96**, 3343-3357, 1991.
- MacIsaac, J. J., and R. C. Dugdale, The kinetics of nitrate and ammonia uptake by natural populations of marine phytoplankton, *Deep Sea Res., Oceanogr. Abstr.*, **16**, 45-57, 1969.
- Mackey, D. J., J. Parslow, H. W. Higgins, F. B. Griffiths, and J. E. O'Sullivan, Plankton productivity and biomass in the western equatorial Pacific: Biological and physical controls, *Deep Sea Res., Part II*, **42**, 499-533, 1995.
- Maes, C., G. Madec, and P. Delecluse, Sensitivity of an equatorial Pacific OGCM to the lateral diffusion, *Mon. Wea. Rev.*, **125**, 958-971, 1997.
- Martin, J. H., Glacial-interglacial CO_2 change: The iron hypothesis, *Paleoceanography*, **5**, 1-13, 1990.
- McCarthy, J. J., C. Garside, J. L. Nevins, and R. T. Barber, New production along 140°W in the equatorial Pacific during and after the 1992 El Niño event, *Deep Sea Res., Part II*, **43**, 1065-1093, 1996.
- McPhaden, M. J., TOGA-TAO and the 1991-93 El Niño-Southern Oscillation event, *Oceanography*, **6**, 36-44, 1993.
- McPhaden, M. J., J. A. Proehl, and L. M. Rothstein, The interaction of equatorial Kelvin waves with realistically sheared zonal currents, *J. Phys. Oceanogr.*, **16**, 1499-1515, 1986.
- Menkes, C., J.-P. Boulanger, and A. J. Busalacchi, Evaluation of TOPEX and basin-wide Tropical Ocean and Global Atmosphere-Tropical Atmosphere Ocean sea surface topographies and derived geostrophic currents, *J. Geophys. Res.*, **100**, 25,087-25,099, 1995.
- Morel, A., Light and marine photosynthesis: A spectral model with geochemical and climatological implications, *Prog. Oceanogr.*, **26**, 263-306, 1991.
- Morel, A., and J.-F. Berthon, Surface pigments, algal biomass profiles, and potential production of the euphotic layer: Relationships reinvestigated in view of remote-sensing applications, *Limnol. Oceanogr.*, **34**, 1545-1562, 1989.
- Moutin, T., and B. Coste, Campagne Océanographique OLIPAC à Bord du N. O. L'Atalante, 3 Novembre - 1er Décembre 1994; Recueil Des Données, data report, 266 pp., Cent. d'Océanol. de Marseille, France, 1996.
- Murray, J. W., R. T. Barber, M. R. Roman, M. P. Bacon, and R. A. Feely, Physical and biological controls on carbon cycling in the equatorial Pacific, *Science*, **266**, 58-65, 1994.
- Murray, J. W., E. Johnson, and C. Garside, A U.S. JGOFS process study in the equatorial Pacific (EqPac): Introduction, *Deep Sea Res., Part II*, **42**, 275-293, 1995.
- Najjar, R. G., J. L. Sarmiento, and J. R. Toggweiler, Downward transport and fate of organic matter in the ocean: Simulation with a general circulation model, *Global Biogeochem. Cycles*, **6**, 45-76, 1992.
- National Oceanic and Atmospheric Administration (NOAA), *Climate Diagnostics Bulletin*, Climate Analysis Center, Washington, D.C., 1994.
- Oudot, C., and Y. Montel, A high sensitivity method for the determination of nanomolar concentrations of nitrate and nitrite in seawater with a Technicon AutoAnalyser II, *Mar. Chem.*, **24**, 239-252, 1988.
- Peña, M. A., M. R. Lewis, and J. J. Cullen, New production in the warm waters of the tropical Pacific Ocean, *J. Geophys. Res.*, **99**, 14,255-14,268, 1994.
- Philander, S. G., *El Niño, La Niña, and the Southern Oscillation*, 293 pp., Academic, San Diego, Calif., 1989.
- Picaut, J., and T. Delcroix, Equatorial wave sequence associated with warm pool displacements during the 1986-1989 El Niño-La Niña, *J. Geophys. Res.*, **100**, 18,393-18,408, 1995.
- Picaut, J., A. J. Busalacchi, M. J. McPhaden, L. Gourdeau, F. I. Gonzalez, and E. C. Hackert, Open-ocean validation of TOPEX/POSEIDON sea level in the western equatorial Pacific, *J. Geophys. Res.*, **100**, 25,109-25,127, 1995.
- Picaut, J., M. Ioualalen, C. Menkes, T. Delcroix, and M. J. McPhaden, Mechanism of the zonal displacements of the Pacific warm pool: Implications for ENSO, *Science*, **274**, 1486-1489, 1996.
- Price, N. M., B. A. Ahner, and F. M. M. Morel, The equatorial Pacific Ocean: Grazer-controlled phytoplankton populations in an iron-limited ecosystem, *Limnol. Oceanogr.*, **39**, 520-534, 1994.
- Radenac, M.-H., and M. Rodier, Nitrate and chlorophyll distributions in relation to thermohaline and current structures in the western tropical Pacific during 1985-89, *Deep Sea Res., Part II*, **43**, 725-752, 1996.
- Raimbault, P., G. Slawycck, B. Coste, and J. Fry, Feasibility of using an automated procedure for the determination of seawater nitrate in the 0-100 nM range: Examples from field and cultures, *Mar. Biol.*, **104**, 347-351, 1990.
- Reynolds, R. W., and T. M. Smith, Improved global sea surface temperature analyses using optimum interpolation, *J. Climate*, **7**, 929-948, 1994.
- Smolarkiewicz, K. P., and T. L. Clark, The multidimensional positive definite advection transport algorithm: Further developments and applications, *J. Comput. Phys.*, **67**, 396-438, 1986.
- Stoens A., C. Menkes, Y. Dandonneau, and L. Mémery, New production in the equatorial Pacific: A coupled dynamical-biochemical model, *Fish. Oceanogr.*, in press, 1998.
- Strickland, J. D. H., and T. Parsons, A practical handbook of seawater analysis, *Fish. Res. Board Can. Bull.*, **167**, 1-310, 1972.
- Tans, P. P., I. Y. Fung, and T. Takahashi, Observational constraints on the global atmospheric CO_2 budget, *Science*, **247**, 1431-1438, 1990.
- Thomas, C., Modélisation tridimensionnelle des champs de nitrate et d'oxygène et de la production nouvelle dans l'Océan Atlantique tropical en 1982-1984, Ph.D. dissertation, 194 pp., Univ. Paul Sabatier, Toulouse, France, 1995.
- Thomas, W. H., Anomalous nutrient-chlorophyll interrelationships in the offshore eastern tropical Pacific Ocean, *J. Mar. Res.*, **37**, 327-335, 1979.
- Toggweiler, J. R., and S. Carson, What are upwelling systems contributing to the ocean's carbon and nutrient budgets?, in *Upwelling in the Ocean: Modern Processes and Ancient Records*, edited by C. P. Summerhayes et al., pp. 337-360, John Wiley, New York, 1995.
- Vialard, J., and P. Delecluse, An OGCM study for the TOGA decade, I, Role of salinity in the physics of the western Pacific fresh pool, *J. Phys. Oceanogr.*, **28**, 1071-1088, 1998a.
- Vialard, J., and P. Delecluse, An OGCM study for the TOGA decade, II, Barrier layer formation and variability, *J. Phys. Oceanogr.*, **28**, 1089-1106, 1998b.

- Walsh, J. J., Herbivory as a factor in patterns of nutrient utilization in the sea, *Limnol. Oceanogr.*, 21, 1-13, 1976.
- Wong, C. S., Y.-H. Chan, J. S. Page, R. D. Bellegay, and K. G. Pettit, Trends of atmospheric CO₂ over Canadian WMO background stations at ocean weather station P, Sable Island, and Alert, *J. Geophys. Res.*, 89, 9527-9539, 1984.
- Wong, C. S., Y.-H. Chan, J. S. Page, G. E. Smith, and R. D. Bellegay, Changes in equatorial CO₂ flux and new production estimated from CO₂ and nutrient levels in Pacific surface waters during the 1986/87 El Niño, *Tellus, Ser. B*, 45, 64-79, 1993.
- Wyrki, K., An estimate of equatorial upwelling in the Pacific, *J. Phys. Oceanogr.*, 11, 1205-1214, 1981.
- Wyrki, K., and B. Kilonsky, Mean water and current structure during the Hawaii-to-Tahiti shuttle experiment, *J. Phys. Oceanogr.*, 14, 242-254, 1984.
- Yentsch, C. S., and D. W. Menzel, A method for the determination of phytoplankton chlorophyll and phaeophytin by fluorescence, *Deep Sea Res., Oceanogr. Abstr.*, 10, 221-231, 1963.
- Yoder, J. A., C. R. McClain, G. C. Feldman, and W. E. Esaias, Annual cycles of phytoplankton chlorophyll concentrations in the global ocean: A satellite view, *Glob. Biogeochem. Cycles*, 7, 181-193, 1993.
-
- J.-M. André and C. Navarette, Centre ORSTOM, BP A5, 98848 Nouméa Cédex, Nouvelle Calédonie, France.
- Y. Dandonneau, N. Grima, L. Mémery, C. Menkès, M.-H. Radenac, and A. Stoens, LODYC, Univ. Pierre et Marie Curie, case 100, 4 place Jussieu, 75252 Paris Cédex 05, France. (e-mail: yd@lodyc.jussieu.fr, mhr@lodyc.jussieu.fr, astlod@ipsl.jussieu.fr, menkes@lodyc.jussieu.fr)
- G. Eldin, Laboratoire d'Etudes en Géophysique et Océanographie Spatiales, 18 avenue Edouard Belin, 31401 Toulouse Cédex 4, France.
- T. Moutin and P. Raimbault, Centre d'Océanologie de Marseille, Campus de Luminy, case postale 901, 13288 Marseille Cédex 09, France.

(Received September 8, 1997; revised August 10, 1998; accepted August 17, 1998.)